Center for Turbulence Research
Proceedings of the Summer Program 2010

Uncertainty quantification for the trailing-edge noise of a controlled-diffusion airfoil

By J. Christophe†, S. Moreau‡, C. W. Hamman, J. A. S. Witteveen AND G. Iaccarino

Two deterministic incompressible flow solvers are coupled with a non-intrusive stochastic collocation method to propagate several aerodynamic uncertainties encountered in a standard trailing-edge noise experiment of a low-speed Controlled-Diffusion (CD) airfoil to predict the far-field noise. Reynolds-Averaged Navier-Stokes (RANS) and Large-Eddy Simulations (LES) are applied to the same restricted domain about the airfoil embedded in the potential core of the jet in the anechoic wind tunnel experiment. Both simulation methods provide the wall-pressure fluctuations near the airfoil trailing edge, which is then used in Amiet's acoustic analogy for trailing-edge noise. In the RANS simulations, two different models are used to reconstruct the wall-pressure fluctuations: Rozenberg's deterministic model directly based on integral boundary-layer parameters, and Panton & Linebarger's statistical model based on the velocity field in the boundary layer. The non-intrusive stochastic model is solved with the inlet velocity profile as random variable. It is found as accurate as and much more efficient than a classical Monte Carlo simulation. The accuracy of the different methods to obtain the wall-pressure spectra is assessed by comparing their mean and standard deviations with experiment.

1. Introduction

In modern rotating machines, significant effort has been gone into reducing or eliminating annoying discrete tones, by either passive devices or active noise control. The next challenge is then to reduce the broadband contribution to decrease the overall noise level and meet new environmental noise regulations. A key source of broadband noise is the trailing-edge noise or self-noise, caused by the scattering of boundary-layer pressure fluctuations into acoustic waves at the trailing edge of any lifting surface. In the absence of any interaction noise source, it represents the dominant source of noise generated by rotating machines such as fans, turboengines (Sharland 1964; Caro & Moreau 2000), wind turbines (Hubbard & Shepherd 1991) and other high-lift devices (Singer *et al.* 2000). A hybrid approach combining a near-field turbulent flow simulation and an acoustic analogy for the sound propagation in the far-field is suitable for broadband noise prediction. The computational cost associated with unsteady turbulent flow simulations still limits most numerical studies to simplified geometries such as airfoils (Wang *et al.* 2004), even with sophisticated non-boundary-conforming methods such as the Lattice Boltzmann method and Immersed Boundary method (Moreau *et al.* 2004), or the use of unstructured grid topologies (Moreau *et al.* 2006a). To meet industrial design constraints, approaches that model the pressure and velocity fluctuations needed for an acoustic analogy from steady RANS are often used (Casalino *et al.* 2010, Glegg *et al.* 2010, Rozenberg *et al.* 2010,

† Von Karman Institute, FRIA fellowship, Brussels, Belgium
‡ Université de Sherbrooke, Sherbrooke QC, J1K2R1, Canada

Remmler *et al.* 2010). These methods add more levels of modeling and the associated epistemic uncertainties grow, which may make the final acoustic prediction inaccurate and unreliable.

Current computational resources are available to perform uncertainty quantification. Aleatoric uncertainty can nowadays have more impact than numerical error and modeling simplifications. The present study aims at assessing only some of the aleatory uncertainties associated with the prediction of trailing-edge noise. In doing so, two different wall-pressure models derived from steady RANS are compared to unsteady LES predictions of the trailing-edge noise for varying inlet velocity profiles. The methodology for uncertainty quantification based on simulations of a standard experimental setup for trailing-edge noise is presented in Sec. 2. The numerical setup and the deterministic flow solvers are summarized in Sec. 3. The stochastic approach is outlined in Sec. 4 and the random variables are described in Sec. 5. The stochastic aerodynamic results are then compared with the available experimental data in Sec. 6 for both flow simulations. The final section assesses the uncertainty on the trailing-edge noise predictions.

2. Methodology for uncertainty quantification

The approach to uncertainty quantification (UQ) of airfoil trailing-edge noise is illustrated in Fig. 1. As in the studies of Wang *et al.* (2004), Moreau *et al.* (2006a) and Christophe & Moreau (2008), a computation of the complete experimental setup of the large anechoic wind tunnel in Ecole Centrale de Lyon (LWT), including the nozzle and part of the anechoic chamber has been done that captures the strong jet-airfoil interaction and its impact on airfoil loading (Moreau *et al.* 2003). The input parameters for this computation are the wind tunnel velocity U_t, air density ρ, and kinematic viscosity ν. The wind tunnel velocity U_t is the main source of uncertainty. Once a value for this parameter is selected, a RANS computation is run on the complete setup and boundary conditions are extracted (U and V profiles) for a smaller domain embedded in the jet potential core as shown in Fig. 2 (a). A second level of uncertainty is introduced by perturbing those profiles to analyze their influence on the final sound prediction. This final result is obtained by two different procedures, both producing a wall frequency pressure spectrum Φ_{pp} used in Amiet's theory to predict the far-field sound spectrum S_{pp}. In the first approach, an unsteady LES on the restricted domain with the above extracted velocity profiles directly yields the trailing edge wall-pressure spectrum. The second approach, less expensive but requiring more modeling, uses steady RANS computations on a two-dimensional slice of the restricted domain, with the same boundary condition profiles as for the LES. From this RANS computation, the primitive variables (U_1, U_2, K and Ω or ϵ depending on the RANS turbulence model) are extracted through a boundary layer profile at the trailing edge of the airfoil. Another way of introducing uncertainty in the complete methodology would be to perturb the boundary layer parameters directly and propagate this uncertainty up to the sound prediction. Those variables are then used in the two wall-pressure models investigated in the present study. On the one hand, Rozenberg *et al.* (2010) proposed a model (YR) based only on global boundary layer parameters from the boundary layer profile, mainly the external velocity U_e, a boundary layer thickness δ or instead the displacement thickness δ^*, and the wall shear stress τ_w. On the other hand, the model of Panton & Linebarger (1974) uses local parameters, i.e., the streamwise velocity profile U_1 and the crosswise velocity fluctuation profile u_2'. A direct comparison of all methods of predicting wall-pressure spectra is made in terms of mean and uncertainty bars and their impact on the radiated sound is evaluated.

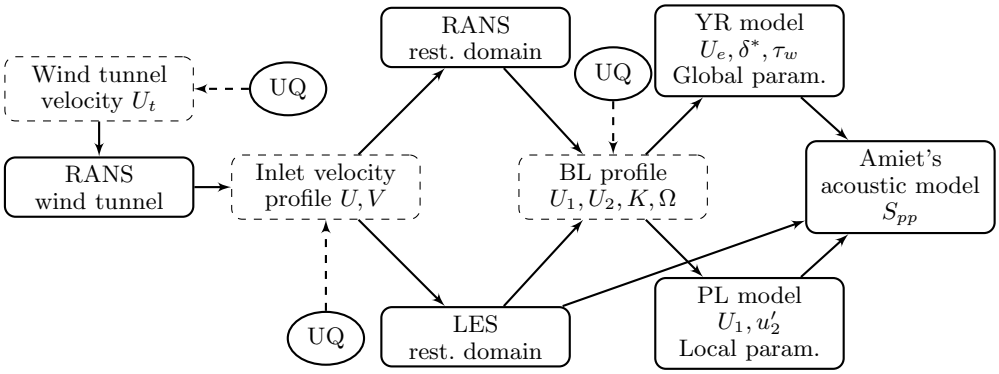

FIGURE 1. Uncertainty quantification methodology

3. Deterministic flow simulations for the CD airfoil

All RANS computations are obtained with the solver Ansys Fluent 12, using the Shear-Stress-Transport (SST) $K-\Omega$ turbulence model developed by Menter (1994). Second-order schemes are used for spatial discretization of all variables. The computational grid is a two-dimensional cut perpendicular to the airfoil span of the structured mesh used by Wang *et al.* (2004). The RANS computations use a no-slip boundary condition on the airfoil surface, a convective outflow boundary condition at the exit plane, and velocities (U and V) from the wind tunnel computation at the inlet. RANS simulations were run until a convergence of the normalized residuals of 10^{-15} was reached.

The LES are solved with CDP (Ham & Iaccarino, 2004). The mesh taken from Moreau *et al.* (2006a) and labeled *CDP-B* has 1.5 million nodes. The same inflow/outflow conditions as for the RANS are used. Periodic boundary conditions are applied in the spanwise direction. For all 9 LES, a dimensionless time step of $2.5 \cdot 10^{-4}$ normalized by the chord C and the reference velocity U_t yields a CFL smaller than one in the whole domain. After a statistically steady state was reached, surface pressure and flow statistics were collected for 50 flow-through times to yield excellent spectral resolution even at low frequencies.

4. Stochastic method

Classical methods for stochastic differential equations rely on Monte Carlo (MC) simulations that prescribe ensemble random inputs to these equations and then collect their ensemble solution realizations. They only require running a deterministic solver repetitively and do not depend on the stochastic dimensionality of the problem; however, they suffer from a slow convergence rate and require a large number of samples, which is prohibitive for turbulent flow realizations. An example of this method is presented below.

Alternative methods are the sensitivity methods based on the moments, the perturbation methods where all stochastic variables are expanded in Taylor expansions around their mean, the stochastic collocation methods, and the spectral or Galerkin projection methods. The first two methods either strongly depend on the modeling assumptions or are limited to small variations. As existing flow solvers are used, non-intrusive stochastic methods are preferred, which means that the projection is not applied to the Navier-Stokes equations directly, but rather to its inputs and outputs. Among the various projection methods, the stochastic collocation expansion (SC) is selected as it has proved its efficiency for flow simulations in various regimes (Babuška *et al* 2007). For instance,

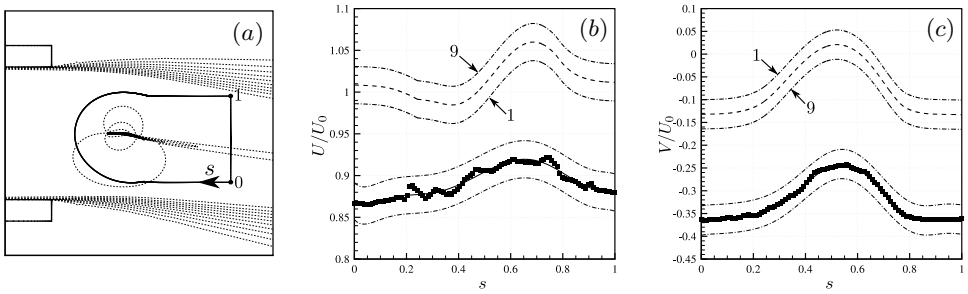

FIGURE 2. (a) Parameterization of inlet boundary condition (solid line) and velocity magnitude contours (dashed line), levels 0-1.7 with increment 0.1. Parametric inlet velocity profiles: (b) streamwise velocity U and (c) crosswise velocity V. (Square) Experimental measurements, (plain) least-squares fit of experimental profiles, (dash) numerical inlet profile extracted from LWT RANS computations and (dash-dot) uncertainty bounds around inlet profiles.

the random wall-pressure spectrum near the trailing edge $\Phi_{pp}(\omega,\theta)$ is expanded as a finite dimensional representation based on a trial basis $\vec{\Psi}(\vec{\xi}(\theta))$ where $\vec{\xi}$ are the random variables, functions of the random parameter $\theta \in [0,1]$:

$$\Phi_{pp}(\omega,\theta) = \sum_{i=0}^{P} \Phi_{pp}^{i}(\omega)\, \Psi_i(\vec{\xi}(\theta)) \tag{4.1}$$

with the deterministic coefficients $\Phi_{pp}^{i}(\omega)$ given by

$$\Phi_{pp}^{i}(\omega) = E\{\Phi_{pp}(\omega,\theta)\, \Psi_i(\vec{\xi}(\theta))\}/E\{\Psi_i^2(\vec{\xi}(\theta))\},$$

where E denotes the expectation. The evaluation of these coefficients is therefore equivalent to computing multidimensional integrals, for which classical quadrature methods are used. Standard Gauss-quadrature requires recomputing each modal coefficient in Eq. (4.1) each time P is increased, which is prohibitive for LES. In the present study, non-intrusive stochastic collocation based on Lagrange interpolation polynomials with Clenshaw-Curtis quadrature points has been applied, allowing both weights and abscissae to be kept when P is varied.

5. Determination of the random variables

Preliminary tests using the wind tunnel velocity U_t as an uncertain parameter showed reduced variations on the far-field sound spectrum, as expected from the weak variation of the RANS solutions in this Reynolds number range. The second method where uncertainty is introduced at the inlet boundary of the restricted computational domain (Fig. 1) is then preferred and the manner of perturbing these profiles is described next.

Figure 2 (a) shows iso-contours of velocity magnitude from a full RANS computation. The wind tunnel velocity was set to the nominal value $U_t/U_0 = 1$. The velocity components (U and V) from this simulation are interpolated on the boundaries of the restricted domain and imposed as inlet conditions. At similar locations, X-wire measurements were performed. Both experimental and numerical velocity components are compared in Fig. 2 as a function of the parametric coordinate. Even if both have similar variations, the experimental profiles exhibit a bias error on the amplitude of both velocity components, which might be caused by a systematic drift in the probe positioning or in the mean

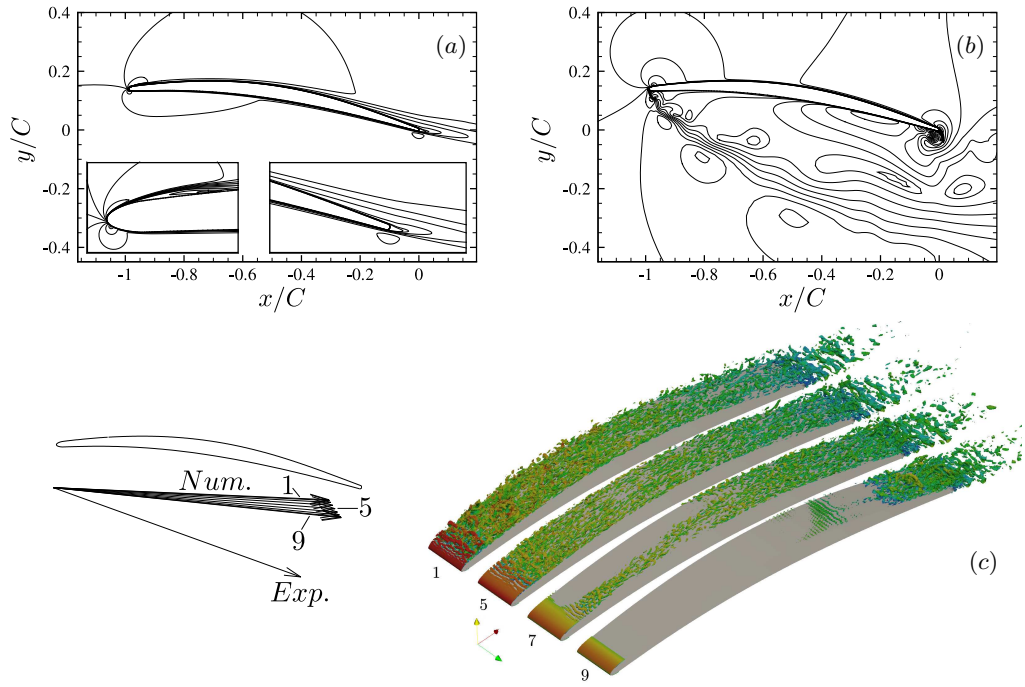

FIGURE 3. Velocity magnitude iso-contours : (a) Reference solution (LES #5) and (b) Experimental inlet conditions (RANS). Contour levels 0-2 with increment 0.1. (c) Iso-surfaces of the Q factor ($Q = 2000\ s^{-2}$) colored by velocity magnitude for inflow conditions corresponding to LES computations # 1,5,7,9.

velocity measurement. If the mean experimental profiles are applied as inlet boundary conditions, the resulting flow field is shown in Fig. 3 (b): an unphysical flow separation is observed at the leading edge on the pressure side, corresponding to a strong negative incidence of the airfoil, as sketched in the center of Fig. 3. The physical variations in the experimental flow measurements are taken into account by selecting a 2.5% error bound on the streamwise velocity U and a 10% error bound on the crosswise velocity V around the deterministic numerical solution from the variations seen in the experimental profiles. The measurement bias error is ignored, since that does not reflect true physical variation (aleatoric uncertainty) in the system, and it would lead to excessive spurious input uncertainty. The upper and lower bounds are shown in Fig. 2, together with the deterministic profiles. From those bounds, a set of 17 then 9 velocity inlet profiles are determined using a Clenshaw-Curtis quadrature. Seventeen RANS and 9 LES corresponding computations are run. Both components U and V are assumed to be random variables with uniform distribution within their interval of variation. The stochastic collocation is found to converge with 9 samples only. As mentioned in Sec. 4, Monte-Carlo simulations of the RANS case have also been carried out to check the accuracy of the SC and demonstrate the highly efficient alternative this method represents. In the selected interval about a thousand samples are needed to statistically converge, which makes the stochastic collocation based on Clenshaw-Curtis quadrature method about two orders of magnitude faster for the present study.

6. Stochastic aerodynamic results

6.1. *Flow topology*

The flow around the airfoil is first described by the velocity magnitude from the LES for the mean incident velocity vectors sketched in Fig. 3. As in previous studies by Wang *et al.* (2004), Moreau *et al.* (2006a) and Christophe & Moreau (2008), the reference case #5 (Fig. 3 (a)) shows a laminar separation bubble at the leading edge that triggers transition, a thickening of the turbulent boundary layer after mid-chord up to the trailing edge without any flow separation. At larger angles of attack, this recirculation bubble increases and the flow remains attached at the trailing edge. For the lowest angles of attack, the laminar recirculation bubble has disappeared at the leading edge but a new one has formed after mid-chord. This is a significant departure from the corresponding RANS solution, which exhibits no recirculation bubble. It should be stressed that this transition in the LES occurs suddenly for a very small variation of incidence in the last two runs (LES #8 and #9). Changes in flow kinematics are described by isosurfaces of Q factor in Fig. 3 (c). In LES #1 and #5 (reference calculation), small instabilities form close to the reattachment point of the laminar recirculation bubble. The flow tends to re-laminarize toward the mid-chord due to the favorable pressure gradient. When this gradient becomes adverse, the turbulent boundary layer thickens again and larger turbulent structures appear near the trailing edge. In LES #7, the acceleration around the leading edge still yields a weak flow separation at the leading edge, which is not strong enough to trigger transition over the whole span. Turbulence only develops over a narrow band, and only the adverse pressure gradient after mid-chord triggers the full transition and turbulence development. In LES #9, the acceleration around the leading edge is no longer strong enough to trigger a flow separation at the leading edge and no transition occurs before mid-chord. Flow separation occurs beyond mid-chord that triggers the transition close to the trailing edge. Weak vortex shedding is seen in the near-wake on the pressure side for all cases. A quantitative estimate of the on-set and length of the recirculation bubbles is found from the wall-friction coefficient for all inflow conditions involved in the SC, and summarized in Tab. 1. Note that the RANS simulations show growing turbulent flow separations at the trailing edge with increasing incidence, whereas the LES do not.

6.2. *Wall-pressure coefficient and boundary-layer profiles*

The UQ results on the wall-pressure coefficient $-C_p$ are shown in Fig. 4. The symbols correspond to the experimental results and the lines to the mean coefficient from the SC. Error bars emphasize the 100% uncertainty interval. In Fig. 4 (left), the two stochastic methods are compared using the RANS data set. Both MC and SC methods agree very well, yielding the same mean solution and almost identical error bars. They both show larger standard deviations in the leading edge region and particularly on the suction side in the recirculation bubble. Even though the uncertainty bars are smaller at the trailing edge, due to the low value of the mean C_p, the local coefficient of the variation is significant . In Fig. 4 (right), the SC for both RANS and LES are compared. The LES yields smaller error bars except in the aft region where the second laminar recirculation bubble occurs for the lowest incidences. If the last two LES results (#8 and #9) were to be removed, the LES would clearly show less uncertainty than the RANS calculations. In regions where the mean simulation result shows a larger difference with respect to the experimental data, the uncertainty bars are also relatively large and account to a large extent for this difference. Both data sets compare to experiments quite well.

	RANS Computations					LES Computations				
	LE		Mid-chord		TE	LE		Mid-chord		TE
Sim.	x_c/C	l/C	x_c/C	l/C	x_c/C	x_c/C	l/C	x_c/C	l/C	x_c/C
1	-0.997	8.2	-	-	-0.129	-0.997	5.8	-		-
2	-0.997	7.4	-	-	-0.117	-0.997	5.5	-		-
3	-0.996	5.9	-	-	-0.083	-0.996	5.2	-		-
4	-0.991	4.1	-	-	-0.025	-0.993	5.1	-		-
5	-0.984	3.1	-	-	-	-0.988	5.5	-		-
6	-0.981	2.6	-	-	-	-0.983	6.2	-		-
7	-0.976	1.7	-	-	-	-0.981	6.5	-		-
8	-	-	-	-	-	-0.976	2.0	-0.341	18.1	-
9	-	-	-	-	-	-	-	-0.337	17.7	-

TABLE 1. Identification of recirculation zones through starting position (x_c/C) and recirculation length (l/C) depending on the region of appearance, at leading edge (LE), after mid-chord (mid-chord) or trailing edge detachment (TE) for all RANS and LES computations.

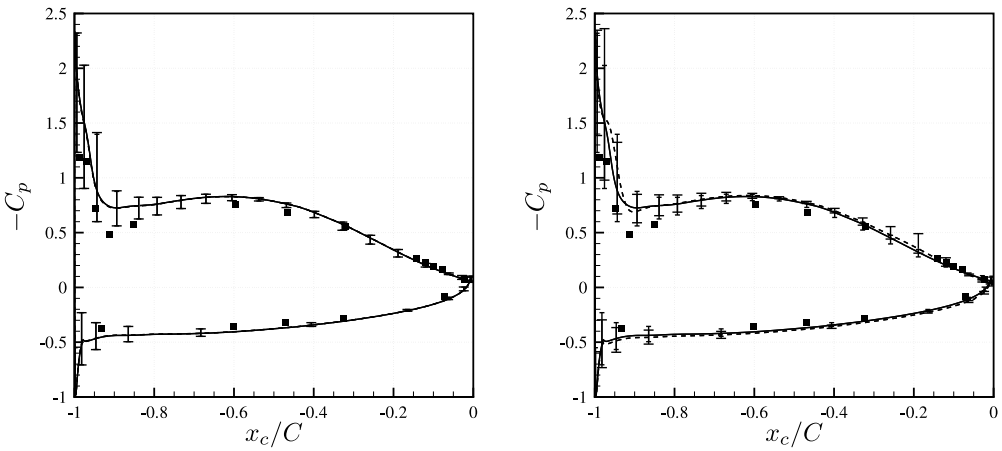

FIGURE 4. Mean wall-pressure coefficient C_p and corresponding uncertainty bars. (Left) Comparison of RANS UQ-based methods: (plain line and small uncertainty bars) SC and (dashed line and large uncertainty bars) MC. (Right) Comparison of flow prediction method using SC: (plain line and small uncertainty bars) RANS computations and (dashed line and large uncertainty bars) LES computations. (Square) Experiments.

Similar UQ results are shown for the boundary-layer velocity profiles in Fig. 5. Special attention is paid to the last remote microphone probe near the trailing edge (RMP #25) as it corresponds to the main source of self-noise noise. In Fig. 5 (left), the two stochastic methods are again compared on the RANS data set. Slightly larger error bars are found for the MC method, which may mean that more samples would be still required. Both mean value profiles compare reasonably well with the hot-wire measurement. The external velocity is lower in the measurements, which hints at a different shear-layer development

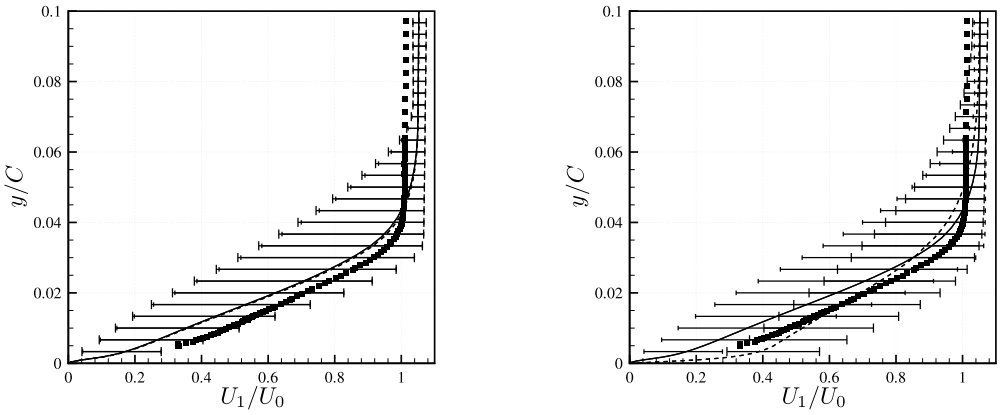

FIGURE 5. Mean streamwise boundary-layer velocity-profile and corresponding uncertainty bars above RMP #25. (Left) Comparison of RANS UQ-based methods: (plain line and small uncertainty bars) SC and (dashed line and large uncertainty bars) MC. (Right) Comparison of flow prediction method using SC: (plain line and small uncertainty bars) RANS computations and (dashed line and large uncertainty bars) LES computations. (Square) Experiments.

and deflection in the experiment. In Fig. 5 (right), the SC for the RANS simulations show significantly larger standard deviations than the SC for the LES. Moreover, the SC for LES is much more centered around the hot-wire experimental data.

From these boundary-layer velocity profiles, the necessary boundary-layer parameters for the consequent models of the wall-pressure spectra can be inferred. Table 2 summarizes the mean and standard deviations obtained for all stochastic methods on both RANS and LES data sets along with the available experimental ones. Excellent agreement is found between the two stochastic methods applied to the RANS results. The largest discrepancies (3%) are found on the parameters describing the effect of the pressure gradients, namely Clauser's local parameter β_C and Coles' global wake parameter Π defined in Sec. 6.3. As Fig. 4 suggests, the LES mean values differ from the RANS ones, especially for the parameters involving the pressure gradient. The corresponding standard deviations are also smaller than the RANS ones. Both data sets agree reasonably well with the experimental data.

6.3. *Wall-pressure statistics near the trailing edge*

In the LES simulations, the wall-pressure statistics at RMP #25 are directly extracted from the simulations. In the RANS, all variables are averaged and the wall-pressure fluctuations are reconstructed from the mean flow. Two such models are considered.

The YR model only uses integrated boundary layer parameters and reads

$$\frac{\Phi_{pp}(\omega)\,U_e}{\tau_w^2\,\delta} = \frac{0.78\,(1.8\,\Pi\,\beta_C + 6)\,\left(\dfrac{\omega\delta}{U_e}\right)^2}{\left[\left(\dfrac{\omega\delta}{U_e}\right)^{0.75} + 0.5\right]^{3.7} + \left[1.1\left(\dfrac{\omega\delta}{U_e}\right)\right]^7}, \tag{6.1}$$

where Clauser's parameter is $\beta_C = (\Theta/\tau_w)(dp/dx)$ and Coles' parameter Π is given by the implicit law of the wake: $2\,\Pi - \ln(1+\Pi) = \frac{\kappa\,U_e}{u_\tau} - \ln\left(\frac{\delta^\star\,U_e}{\nu}\right) - \kappa\,C - \ln\kappa$. For Eq. (6.1), the original expression based on δ has been preferred to the formulation recently

	RANS SC		RANS MC		LES SC		Experiments
Parameter	Mean	Std	Mean	Std	Mean	Std	Mean
U_e [m/s]	16.35	0.16	16.36	0.16	15.92	0.23	16.09
δ_{95} [mm]	5.60	1.30	5.52	1.25	5.95	1.79	5.36 (δ_{99})
δ^* [mm]	2.36	0.70	2.32	0.68	1.86	0.61	1.83
Θ [mm]	0.89	0.18	0.88	0.18	0.98	0.30	0.79
τ_w [Pa]	0.29	0.08	0.28	0.07	0.61	0.11	-
U_τ [m/s]	0.48	0.07	0.48	0.07	0.70	0.06	-
β_C	7.89	2.34	8.11	2.37	4.89	1.75	-
Π	3.26	1.01	3.34	1.00	0.53	0.22	-

TABLE 2. Boundary layer parameters (mean and standard deviation) for RANS computations using SC or MC and LES computations using SC.

proposed by Rozenberg *et al.* (2010) based on $\delta^\star$, as it provides a better agreement with the experimental data for the CD airfoil. As explained by Rozenberg *et al.* (2010), the friction velocity u_τ is obtained from extended Clauser plots rather than from direct upwind finite-difference estimates. Similarly, the wake law is also verified graphically by comparing the model with the measured dimensionless velocity log plots (u^+, y^+).

Using the PL model (Panton, 1974), Remmler *et al.*(2010) derived an expression for the wall-pressure spectrum

$$\Phi_{pp}(\omega) \;=\; 8\,\rho^2 \iiint_0^\infty \frac{k_1(\omega)^2}{k(\omega)^2}\; \exp^{-k(\omega)(y+\hat{y})}\; S_{22}(y,\hat{y},\omega)\,\frac{\partial U_1}{\partial y}\,\frac{\partial U_1}{\partial \hat{y}}\,dy\,d\hat{y}dk_3, \qquad (6.2)$$

with the energy spectrum of the vertical velocity fluctuations

$$S_{22}(y,\hat{y},\omega) \;=\; \frac{\bar{u_2'}(y)\,\bar{u_2'}(\hat{y})}{\pi^2}\,\Lambda^2 \iint_0^\infty R_{22}\cos(\alpha\,k_1(\omega)\,r_1)\;\cos(\alpha\,k_3\,r_3)\,dr_1\,dr_3.$$

The model therefore uses the streamwise mean velocity profile $U_1(y)$ and the crosswise velocity fluctuation profile $u_2'(y)$. Both velocities and the turbulence integral length scale Λ are calculated from the RANS outputs. The velocity correlation function R_{22} and the scale anisotropy factor α need to be modeled. No quadratures are used to calculate the quintuple integral in Eq. (6.2) as they would require a prohibitive amount of memory. The integration is performed with a Monte Carlo method using importance sampling for enhancing convergence. More details on this model can be found in Remmler *et al.* (2010).

The UQ results for the YR model are shown in Fig. 6 (a). Good agreement is found between the mean wall-pressure spectrum and the measured one at RMP #25. Significant standard deviations are found at high frequencies, whereas limited ones are seen at low frequencies, which makes this model quite robust for the prediction of the overall trailing-edge noise level. At high frequencies, the large error bars are induced by the large uncertainty on the wall shear-stress. In Fig. 6 (b) the UQ results for the PL model show a similar agreement between the mean value and the measured spectrum and a similar crossing with almost no error bar around 1 kHz. The standard deviations are smaller at high frequencies for the PL model than with the YR model as this model does not

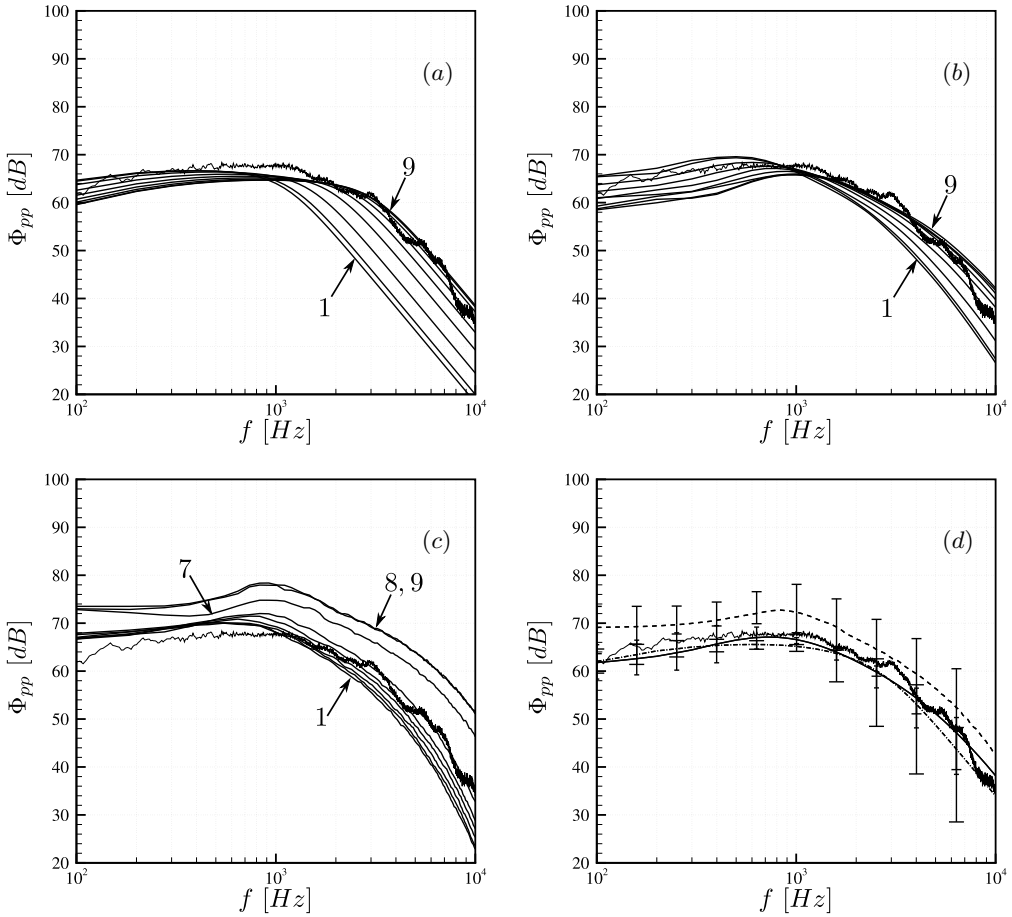

FIGURE 6. Wall-pressure frequency spectra in the leading edge area ($x_c/C = -0.02$, RMP # 25) using (a) Rozenberg's model and (b) using Panton & Linebarger's model for all RANS computations. (c) LES wall-pressure spectra. (d) Comparison of wall-pressure spectra based on RANS and LES inputs in terms of mean and uncertainty bars, (dash-dot and large uncertainty bars) Rozenberg's model, (plain and small uncertainty bars) Panton & Linerbarger's model, (dash and medium uncertainty bar) LES. (Thin plain) Experiments.

directly depend on the wall shear-stress. Yet, at low frequencies, they are larger mainly because of the slow statistical convergence of the Monte-Carlo integration technique used in Eq. (6.2). Excellent statistical convergence of all LES runs is achieved, which provides a low-frequency resolution better than the one achieved by Moreau *et al.* (2006a). In Fig. 6 (c) two groups of LES results are obtained. On the one hand, the LES #1 to #6 are similar to the reference calculation (LES #5) and show similar variations as the RANS. On the other hand, the LES #7 to #9 show a recirculation bubble close to the trailing edge triggering larger pressure fluctuations for all frequencies. Consequently, in Fig. 6 (d) the mean pressure spectrum in the SC of the LES is shifted to higher levels by about 8 dB, and the standard deviations are larger. Yet the latter are still smaller than for both RANS methods, especially if the last two simulations are discarded.

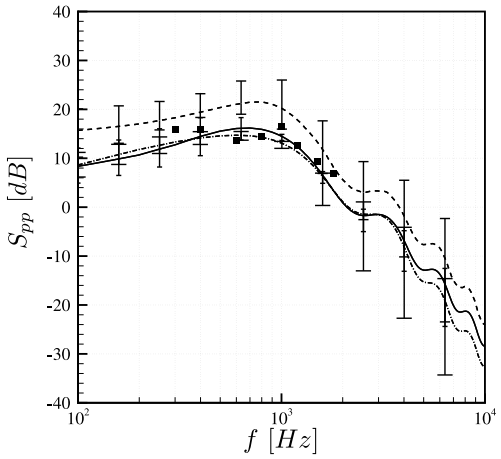

FIGURE 7. Means and uncertainty bars of far-field acoustic spectra for the different methods, in the mid-span plane above the airfoil ($\theta = 90°$) at R = 2 m from the trailing edge. (Dash-dot and large uncertainty bars) Rozenberg's model, (plain and small uncertainty bars) Panton & Linerbarger's model, (dash and medium uncertainty bar) LES. (Square) Experiments.

7. Stochastic acoustic predictions

As shown by Roger & Moreau (2005), the trailing-edge noise can be obtained by iteratively solving scattering problems at the airfoil edges. The random predicted sound field in the midspan plane at a given observer location $\vec{x} = (x_1, x_2, 0) = (R, \theta, z = 0)$ and for a given radian frequency ω (or wavenumber k) then reads

$$S_{pp}(\vec{x}, \omega, \theta) \;=\; p_a(\vec{x}, \omega, \theta)\, p_a^{\star}(\vec{x}, \omega, \theta) \;=\; \left(\frac{\sin\theta}{2\,\pi\,R}\right)^2 (k\,c)^2\,\frac{L}{2}\,|I|^2\,\Phi_{pp}(\omega, \theta)\,l_y(\omega), \tag{7.1}$$

where Φ_{pp} is the random wall-pressure power spectral density defined in Sec. 4 and l_y the spanwise correlation length near the trailing edge is assumed to be deterministic. The radiation integral I involving both the free stream velocity U_∞ and the convection speed as parameters can be found in Roger & Moreau (2005). In Fig. 7 the mean results compare favorably with the experimental far-field sound. Similar uncertainty propagation is seen at both low and high frequencies for the RANS simulations. The YR model is again better at low frequencies, whereas the PL is better at high frequencies. The LES SC has larger error bars mainly caused by the runs #7 to #9 for which there is an additional flow separation, and that creates a biased spreading of the results.

8. Conclusions

The uncertainty quantification framework has been successfully applied to the broadband trailing-edge noise of a CD airfoil at moderate angle of attack (8°). Uncertainty is introduced as random velocity components at the inlet of the restricted computational domain embedded in the potential core of the jet of a typical aeroacoustic experiment on trailing-edge noise. These random variables are intended to model the experimental uncertainty in the probe position and in the measurement of the reference velocity, and the numerical inaccuracies in the prediction of the jet development and deflection. Two deterministic incompressible flow solvers have then been coupled with a non-intrusive

stochastic Galerkin method based on a SC to propagate these aerodynamic uncertainties. Unsteady turbulent flow predictions are provided by incompressible LES and the steady ones by RANS simulations using the $k-\omega$ SST turbulence closure model. The former directly provide the wall-pressure fluctuations near the trailing edge, which are then used in Amiet's acoustic analogy for the prediction of trailing-edge noise. In the latter, two different models are used to reconstruct the wall-pressure fluctuations: the deterministic YR model directly based on the wall-pressure statistics and the PL statistical model based on the velocity field in the boundary layer.

The convergence of the SC based on the RANS data set has been verified by extending the number of terms in the Curtis-Clenshaw sparse quadrature and by comparing with a Monte Carlo simulation. Its efficiency is clearly demonstrated as it provides the same accuracy with a limited number of terms (9) and is two orders of magnitude faster. The same number of terms has been kept in the SC based on the LES data. Several differences are noticeable in the flow topology associated with both types of simulations. In the LES, at the lowest angles of attack, the laminar recirculation bubble at the leading edge disappears and a new one forms in the aft of the airfoil. The latter triggers an 8 dB increase in the wall-pressure spectra near the trailing-edge. As a consequence, the LES-SC has larger standard deviations than the RANS-SC in the wall-pressure spectra and consequently in the far-field noise over most frequencies, whereas it has clearly smaller error bars in the boundary-layer velocity profiles. If the last two simulations were discarded, the LES would trigger lower standard deviations overall. When comparing both RANS-SC, both YR and PL models yield very small error bars around 1 kHz. The YR model has large increasing standard deviations at high frequencies caused by its strong dependence on the random wall shear-stress that has a broad probability density function and carries large uncertainties. On the contrary, the PL model has much smaller error bars at high frequencies but carries more uncertainty at the low frequencies caused by the slow convergence of the Monte Carlo technique used in this model. For overall sound pressure levels, the YR model thus appears more reliable. The mean values of all SC compare well with experimental data.

Finally, uncertainty could also have been introduced on the global parameters of the boundary layer or on the local velocity profiles. Epistemic uncertainties also exist in the turbulence close models of the RANS and in the actual form of the functions accounting for turbulence anisotropy (R_{22} and α in PL model) or for the pressure gradients (the linear term in Π and β_C in the YR model) in the wall-pressure models. The use of an inverse UQ method could also be considered to get more realistic random inlet inputs and prevent the bias introduced by the lowest two angles of attack in the LES-SC. A new set of experimental data should also be collected around the CD airfoil to provide more reliable velocity components on the boundaries of the computational domain.

Acknowledgments

The authors would like to thank Professor Parviz Moin for providing the necessary computational resources on the Certainty cluster and Dr. Yaser Khalighi for providing the reference CDP solution on the CD airfoil. The participation of the first author to the Summer Program has been supported through the FP7-ECOQUEST project (Grant Agreement no 233541) and AETHER project (contract no MRTN-CT-2006-035713).

REFERENCES

Babuška, I., Nobile, F. & Tempone, R. 2007 A stochastic collocation method for elliptic partial differential equations with random input data. *SIAM J. Numer. Anal.* **45**(3), 1005–1034.

Caro, S. & Moreau, S. 2000 Aeroacoustic modeling of low pressure axial flow fans. *AIAA Paper 2000-2094*, Sixth AIAA/CEAS Aeroacoustics Conference, Lahaina, Hawaii. June 12–14.

Casalino, D., Moreau, S. & Roger, M. 2010 Trailing edge noise measurements and prediction for a subsonic loaded fan blade. *International J. Aeroacoustics* **9**(3), 307–327.

Christophe, J. & Moreau, S. 2008 LES of the trailing-edge flow and noise of a Controlled-Diffusion airfoil at high angle of attack. *Proceedings of the Summer Program 2008*, Center for Turbulence Research, Stanford Univ./NASA Ames.

Glegg, S., Morin, B., Atassi, O. & Reba, R. 2010 Using Reynolds-Averaged Navier-Stokes calculations to predict trailing edge noise. *AIAA J.* **48**(7), 1290–1301.

Ham, F. & Iaccarino, G. 2004 Energy conservation in collocated discretization schemes on unstructured meshes. *Annual Research Briefs-2004*, Center for Turbulence Research, Stanford Univ./NASA Ames.

Hubbard, H. H. & Shepherd, K. P. 1991 Aeroacoustics of large wind turbines. *J. Acoust. Soc. Am.* **89**, 2495–2507.

Menter, F. R. 1994 Two-equation eddy-viscosity turbulence models for engineering applications. *AIAA J.* **32**(8), 1598–1605.

Moreau, S., Henner, M., Iaccarino, G., Wang, M. & Roger, M. 2003 Analysis of flow conditions in free-jet experiments for studying airfoil self-noise. *AIAA J.* **41**(10), 1895–1905.

Moreau, S., Iaccarino, G., Kang, S., Khalighi, Y. & Wang, M. 2004 Towards a large eddy simulation of a low speed fan blade. *Proceedings of the Summer Program 2004*, Center for Turbulence Research, Stanford Univ./NASA Ames.

Moreau, S., Neal, D., Khalighi, Y., Wang, M. & Iaccarino, G. 2006a Validation of unstructured-mesh LES of the trailing-edge flow and noise of a controlled-diffusion airfoil. *Proceedings of the Summer Program 2006*, Center for Turbulence Research, Stanford Univ./NASA Ames.

Panton, R. L. & Linebarger J. H. 1974 Wall pressure spectra calculations for equilibrium boundary layers. *J. Fluid Mech.* **65**, 261–287.

Remmler, S., Christophe, J., Anthoine, J. & Moreau, S. 2010 Computation of wall-pressure spectra from steady flow data for noise prediction. *AIAA J.* **48**(9), 1997–2007.

Roger, M. & Moreau, S. 2005 Back-scattering correction and further extensions of Amiet's trailing edge noise model. Part 1: theory. *J. Sound Vib.* **286**(3), 477–506.

Rozenberg, M., Moreau, S., Henner, M. & Morris, S. C. 2010 Fan trailing-edge noise prediction using RANS simulations. *AIAA Paper 2010-3720*, Sixteenth AIAA/CEAS Aeroacoustics Conference, Stockholm, Sweden. June 7–9.

Sharland, I. J. 1964 Sources of noise in axial flow fans. *J. Sound Vib.* **1**(3), 302–322.

Singer, B. A., Lockard, D. P. & Brentner, K. S. 2000 Computational aeroacoustic analysis of slat trailing-edge flow. *AIAA J.* **38**(9), 1558–1564.

Wang, M., Moreau, S., Iaccarino, G. & Roger, M. 2004 LES prediction of wall pressure spectra on a low speed airfoil. *Annual Research Briefs-2004*, Center for Turbulence Research, Stanford Univ./NASA Ames.